buildings

MDPI

Article

Shaking Table Test and Numerical Simulation Study of the Reinforcement Strengthening of a Dam

Qiang Xu [1], Bo Liu [1,*], Jianyun Chen [1], Jing Li [1] and Mingming Wang [2]

[1] State Key Laboratory of Coastal and Offshore Engineering, Dalian University of Technology, Dalian 116024, China
[2] Faculty of Electric Power Engineering, Kunming University of Science and Technology, Kunming 650500, China
* Correspondence: liubo2221@mail.dlut.edu.cn

Abstract: This paper presents experimental and numerical investigations of the seismic failure of the reinforced and unreinforced monoliths of the Huangdeng concrete gravity dam. To verify the scale factors, we use suitable materials (emulation concrete material and fine alloy wire) to simulate the dam concrete and the steel reinforcement (SR) in a scaled experiment model that includes the water-retaining monolith and overflow monolith of the dam. We design shaking table model tests based on the similarity laws and perform nonlinear numerical simulations of damage to the dam. By comparing the numerical simulation with the experimental results, the intervals for peak acceleration, in which microcracks appear and macrocracks rapidly expand, are obtained. The modal and damage distribution results verify the proposed design method for the scaled experimental model with SR. By analyzing the results, we reveal the crack resistance mechanism of SR. This research provides a rational foundation for further study of the similarity laws for reinforced dams.

Keywords: gravity dam; reinforced steel; shaking table model test; similarity laws; numerical simulation

check for updates

Citation: Xu, Q.; Liu, B.; Chen, J.; Li, J.; Wang, M. Shaking Table Test and Numerical Simulation Study of the Reinforcement Strengthening of a Dam. *Buildings* **2022**, *12*, 1955. https://doi.org/10.3390/buildings12111955

Academic Editor: Giovanni Minafo

Received: 3 October 2022
Accepted: 9 November 2022
Published: 11 November 2022

1. Introduction

Many high concrete gravity dams are under construction or will soon be built in southwestern China, where high-intensity earthquakes frequently occur. Some of these dams are 200-m high, making them the highest concrete gravity dams in the world. The aseismic design of high concrete dams is important. Embedding steel reinforcement (SR) in dam concrete is a common reinforcement measure for concrete dams. At present, the shaking table test and numerical simulation are mainly used to predict the seismic response of reinforced concrete dams.

In the research of model tests of concrete gravity dams, many investigators have studied small-scale experimental models on shaking tables to simulate kinematic failure [1–3] and explored the seismic crack propagation pattern of the dams [4–6]. Zhao simulated the reinforced concrete part of the dam by increasing the elastic modulus of the model material, and the seismic experiment of concrete gravity dams is carried out; however, this study could not obtain a similar scale between the dam prototype and the experimental model [7]. To simulate the influence of SR, Wang et al. [8] proposed a model test design method that enables concrete gravity dams to be tested on a shaking table with water. The results show that the reinforcement has a certain restriction on the development of the main crack.

In addition, the use of numerical simulations to analyze the damage of structures under strong seismic effects is also very common [9–11]. To numerically simulate the damage to concrete gravity dams under ground motion, many investigators have used discrete crack models [12,13] or smeared crack models [14,15] in the framework of continuum mechanics [16–18]. In addition to those models, the extended finite element method, the crack-embedded element method [19], the discrete element method [20], discontinuous deformation analysis [21], and the failure process model for rock [22] are typical models of crack propagation that are applicable to concrete dams. To simulate the influence of SR and tension on the structural stiffness of the dam concrete, Long et al. [23] analyzed stiffening reinforced steel [24] with a zoning method [25] and presented a modified embedded-steel model.

Other studies have compared the results of scaled experimental models and numerical prototype models of concrete gravity dams. Hariri [26] compared the seismic cracks of a gravity dam based on numerical simulation and shaking table test. Zhong et al. [27] and Philippe et al. [28] compared the damage results for a gravity dam based on a seismic numerical method and the responsive shaking table test. At present, experimental and numerical studies of shaking tables for gravity dams in concrete are relatively mature. However, there are relatively few studies on the damage mechanism of the reinforced concrete gravity dams under strong seismic effects. In order to effectively conduct shaking table experimental studies on reinforced concrete gravity dams, it is necessary to investigate the similarity relationship of steel reinforcement in the prototype and scale models.

In order to further study the dynamic failure mechanism of reinforced concrete gravity dams under the action of strong earthquakes, we respectively push the similar scales between the dam prototype and structural model, and use suitable materials (emulation concrete material and fine alloy wire) to simulate the dam concrete and the steel reinforcement (SR) in a scaled experiment model that includes the water-retaining monolith and overflow monolith of the dam. The similarity relation of steel frame is derived based on the similarity relation of concrete. Then, numerical simulations were carried out on the reinforced and unreinforced dam prototypes. The results of the numerical simulation of the dam prototype and the structural scale model test show that: the SR similarity requirements and other similarity laws proposed in this paper can obtain accurate natural frequencies, and the prototype numerical results are similar to the results of the scale test in terms of damage, which prove the feasibility of the scheme proposed in this study. In addition, the frequency, acceleration, strain and damage form of the dam model are also analyzed to evaluate the reinforcement effect.

2. The Shaking Table Test

2.1. Experimental Materials

We used simulated concrete material (ECM) as the material of the test model to simulate the dam concrete. ECM has the characteristics of high early strength. Table 1 gives the mixing ratio of various materials of ECM.

Table 1. The mixing ratio of various material.

Water (%)	Cement (%)	Ore Powder (%)	Barite Powder (%)	Barite Sand (%)
9.00	1.50	10.00	30.00	49.50

The compressive strength of ECM is 0.7 MPa~0.8 MPa, and the tensile strength is 30 kPa~60 kPa. The dynamic elastic modulus of ECM is 350 MPa~980 MPa. Furthermore, ECM has a stress-strain curve similar to that of common concrete, as shown in Figure 1. More test details are found in the literature [29,30]. The material damping ratio of ECM is less than 5%. Furthermore, the dynamic elastic modulus of the ECM can be obtained by Equation (1).

$$w_1 = (1.875)^2 \sqrt{\frac{E_E I_E}{\rho_E A_E {L_E}^4}} \tag{1}$$

where the subscript E represents the ECM cantilever beam specimens. Furthermore, L, ρ, and E are the lengths, mass density, and dynamic elastic modulus of the ECM cantilever beam specimens, respectively. A is the cross-sectional area. I is the moment of inertia of the cross section. w_1 is the 1st natural circular frequency of the cantilever beam.

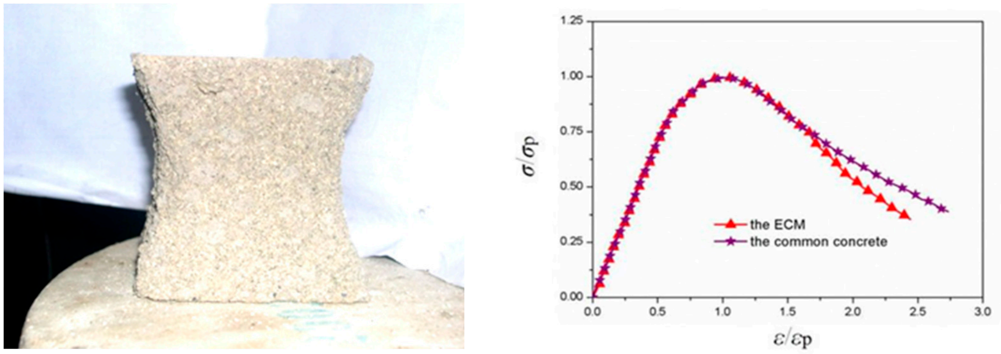

(**a**) ECM specimen (**b**) Normalized compressive stress-strain curves

Figure 1. Experimental materials.

2.2. Similitude Requirements

2.2.1. Dynamic Experiment Involving a Small-Scale Dam Model

In this study, the similarity relationship between the prototype structure and the scale model is derived based on the similarity transformation, as follows.

For the structural damage dynamic test of small dam models, the following similar scales must be satisfied.

$$T_r^2 = L_r^2 \rho_r / E_r \tag{2}$$

$$T_r = \sqrt{\varepsilon_r L_r} \tag{3}$$

$$L_r = \varepsilon_r E_r / \rho_r \tag{4}$$

where T_r is the time scale, L_r is the length scale, ρ_r is the density scale, E_r is the elastic modulus scale, and ε_r is the strain scale. If two of Equations (2) and (3) and Equations (3) and (4) are satisfied, the third equation is automatically satisfied.

Based on the similarity laws,

$$\varepsilon_r = 1 \tag{5}$$

and Equation (3) can be rewritten as follows.

$$T_r = \sqrt{L_r} \tag{6}$$

Additionally, we can obtain the following relations:

$$\sigma_r = E_r = L_r \rho_r \tag{7}$$

$$a_r = 1 \tag{8}$$

$$f_r = 1/T_r \tag{9}$$

where σ_r is the stress scale, a_r is the acceleration scale, and f_r is the frequency scale.

2.2.2. Dam Concrete Similitude Requirements

Because concrete is mainly damaged by tension, when the ε_r = 1, we can obtain the following relation:

$$(f_t)_r = (E_C)_r = L_r (\rho_C)_r \tag{10}$$

where $(f_t)_r$ is the tensile strength scale. The subscript C represents the dam material. As shown in Figure 2, the age of the experimental material (the ECM) can be obtained by Equation (10).

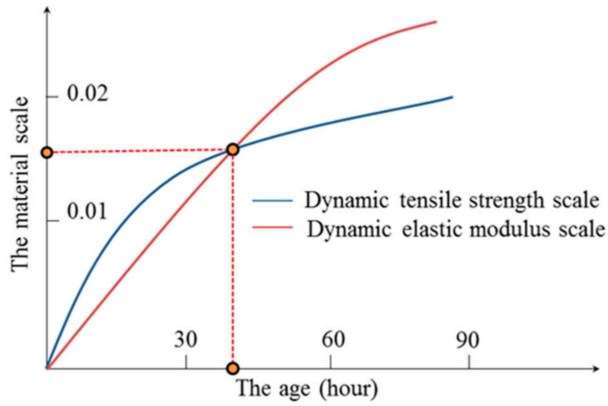

Figure 2. Method for determining the age of the experimental material(s).

Additionally, Equation (10) can be rewritten:

$$L_r = (f_t)_r/(\rho_C)_r = (E_C)_r/(\rho_C)_r \tag{11}$$

Based on Equation (11), the length scale L_r can be determined. Furthermore, other scales can be obtained with Equations (6)–(9).

2.2.3. SR Similitude Requirements

Due to the low SR ratio of most concrete gravity dams, the inertia of the SR can be ignored. It is assumed that the ratios of the loads on the dam concrete and SR between the prototype structure and scaled model are the same.

$$\frac{(F_S)_p}{(F_C)_p} = \frac{(F_S)_s}{(F_C)_s} \tag{12}$$

where F represents the external forces. The subscript p represents the dam prototype. The subscript s represents the test model. The subscripts C and S represent the dam concrete material and SR, respectively. Equation (12) can be rewritten as follows.

$$(F_C)_r = \frac{(F_C)_s}{(F_C)_p} = \frac{(F_S)_s}{(F_S)_p} = (F_S)_r \tag{13}$$

Because the peak tensile strain of the SR is more than 10 times that of concrete, the SR is always in the linear elastic stage when the dam concrete undergoes tensile damage. Futhermore, in the linear elastic stage, the external force scales of the concrete material and SR satisfy the following equations:

$$(F_S)_r = (E_S)_r \times (\varepsilon_S)_r \times (A_S)_r \tag{14}$$

$$(F_C)_r = (E_C)_r \times (\varepsilon_C)_r \times (A_C)_r = (E_C)_r \times (\varepsilon_C)_r \times L_r^2 \tag{15}$$

where A represents the area. It is assumed that there is no slip between the SR and dam concrete. Thus, when $(\varepsilon_s)_r = (\varepsilon_c)_r = 1$, we can obtain the cross-sectional area scale $(A_S)_r$ of the SR of the dam, as follows.

$$(A_S)_r = (E_C)_r \times L_r^2/(E_S)_r \tag{16}$$

Based on Equation (12), the cross-sectional area of the experimental materials used for the SR in the dam can be determined.

2.3. Test Model of Huangdeng Gravity Dam

The Huangdeng Gravity Dam, situated in the upstream area of the Lancang River in China, has a dam length of 203 m and a width of 464 m. There are 20 monoliths for the dam. The water-retaining monolith (WRM) and the overflow monolith (OM) of the Huangdeng gravity dam are analyzed in this paper. The material for the scale model of the dam was ECM, of which the geometric scale was L_r = 1:100. The thickness of the scaled dam model was 20 cm. The scaled dam model and reinforcement diagram are shown in Figure 3. Measuring points are marked in Figure 3b. The dynamic dam model experiment was conducted by using the shaking table facility at the State Key Laboratory of Coastal and Offshore Engineering at Dalian University of Technology, China. The shaking table (digitally controlled) can input three-dimensional (horizontal + vertical + pitch) excitation. The working area of the shaking table measured 4 m × 3 m, and the maximum load capacity was 10 t, while the maximum horizontal and vertical acceleration were 1.0 g and 0.7 g, respectively. The operating frequency range was 0–50 Hz. The control mode was digital control. The shaking direction was "horizontal + vertical + pitch". More details are given in [31]. The scale factors included in the seismic response analysis are shown in Table 2. The material parameters of ordinary concrete and ECM are shown in Table 3. The use time of ECM was 40 h, so as to calculate its elastic modulus. The damping ratio of the ECM was 0.051 and the damping ratio of the concrete was 0.026. The dynamic Young's modulus of the SR was 200 GPa. The dynamic Young's modulus of the fine alloy wire (FAW) was 24 GPa. The Poisson's ratio of the SR was 0.3, and the Poisson's ratio λ of the FAW was 0.28. A video of the dam model can be downloaded through the following link: https://www.dropbox.com/s/yviug8z9qefgl7i/Video%20of%20shaker%20experiment.MPG?dl=0 (Accessed date: 27 October 2022).

Table 2. The scale factors included in the seismic response analysis.

L_r	T_r	$(dT)_r$	ω_r	a_r	ε_r	$(E_s)_r$	$(A_s)_r$	$(\sigma_c)_r$	$(\sigma_s)_r$
1:100	0.1	0.1	10	1	1	0.1205	1:95000	0.012	0.1205

Table 3. The material parameters.

Material Scaler	$(\rho_c)_r$	$(f_t)_r$	$(E_c)_r$	$(\lambda_c)_r$
	1.188	0.012	0.012	0.9
Concrete	Density ρ (kg/m^3)	Dynamic tensile strength f_t (MPa)	Dynamic Young's modulus E (GPa)	Poisson's ratio λ
	2400	3.040	30	0.2
ECM	Density ρ (kg/m^3)	Dynamic tensile strength f_t (MPa)	Dynamic Young's modulus E (GPa)	Poisson's ratio λ
	2850	0.0365	0.36	0.18

The design response spectrum of the prototype of the Huangdeng concrete gravity dam structure was adopted as the standard spectrum based on the Chinese code for seismic design of hydraulic structures in hydropower projects (NB 35047-2015,2015), which was converted into that of the scale dam model by the time scale T_r [32]. Then, the input artificial dynamic history of the scaled dam model was generated by the design response spectrum of the scaled dam model. In addition, the input vibration signal of model is shown in Figure 3c. The progressive loading method was used to input the vibration signal until the model structure was damaged. The peak of acceleration values of the shaking table are shown in Figure 3. The peak acceleration in the vertical direction was 2/3 of that in the horizontal direction. The experimental instruments were a "DSPS" data signal acquisition and processing system, a "PXI-1044" acquisition system, a "SI-425" demodulator, a "AR-5F" acceleration sensor, a laser position measuring instrument, and a fiber grating sensor. The time course of the strain response of the dam in some experiments is shown in Figure 3b.

(**a**) The Huangdeng concrete gravity dam

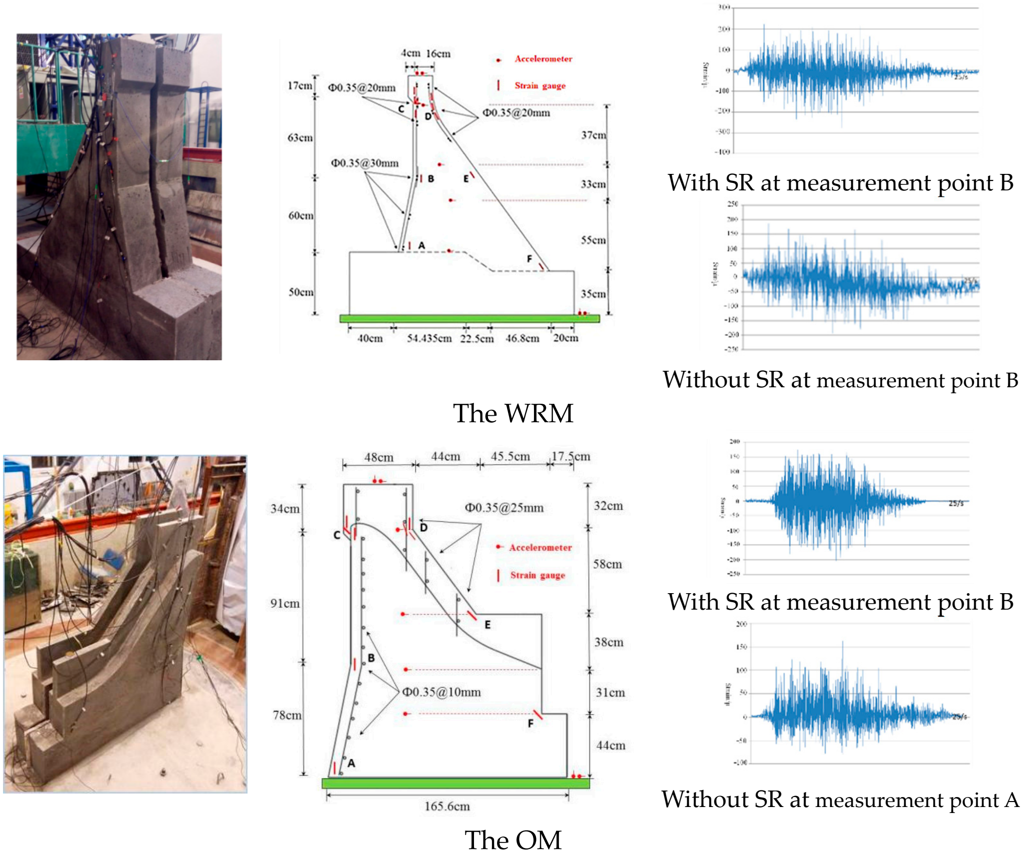

(**b**) The scaled model and the strain response

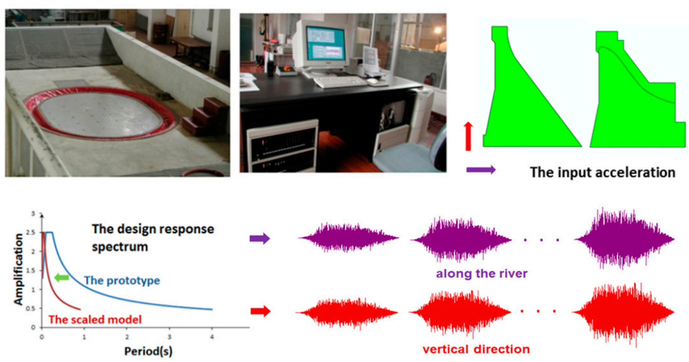

(**c**) The acceleration

Figure 3. The test model of Huangdeng gravity dam.

2.4. Results

Figure 4 shows that the natural frequencies of the WRM- and OM-scaled models start to change when the peak acceleration reaches approximately 0.25 and 0.30 g. The results indicate that the peak accelerations associated with microcrack appearance in the WRM and the OM models on the shaking table are approximately 0.25 and 0.30 g. In the literature [8], the results of shaking table experimental studies on reinforced concrete gravity dams showed that the model stiffness decreased rapidly when the PGA reaches 0.285 g. In [31], the results of shaking table experiments on the overflow section of a high gravity dam showed that the model was significantly damaged when the PGA was greater than 0.316. The results of this study are similar to those in the literature [8,31]. In addition, the results also suggest that the aseismic stability of the OM is higher than that of the WRM. The role of SR is mainly to prevent macrocracks from extending, and the SR has little effect on the formation of microcracks. This role of SR in preventing macrocrack extension is more obvious in the OM.

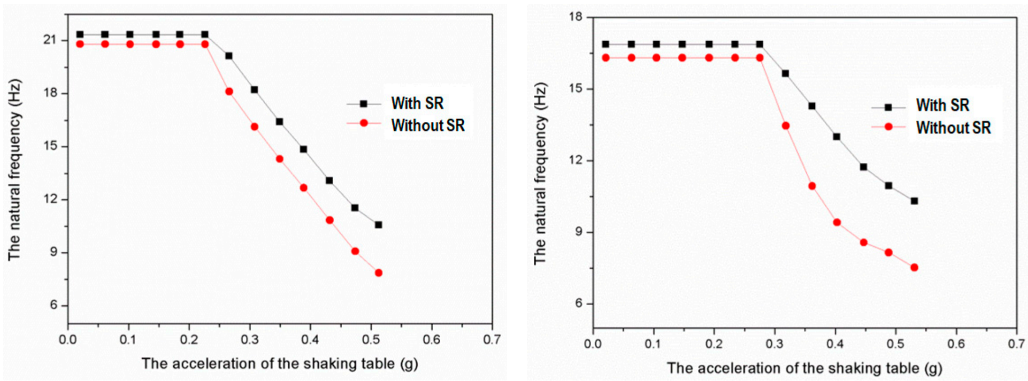

(**a**) The WRM model (**b**) The OM model

Figure 4. The variation of natural frequency with acceleration.

As can be seen from Figure 5, when the peak acceleration is between 0.31 and 0.36 g, the acceleration magnification obviously changes with the distribution of WRM and OM model height. The distributions of amplification based on the heights of the WRM- and OM-scaled models display a very dramatic change before the peak acceleration of the shaking table reaches 0.51 g and 0.53 g, respectively. The results indicate that crack propagation will lead to changes in the distribution of amplification with height for the WRM and OM models. Furthermore, the results illustrate that the peak accelerations for macrocracks to appear in the WRM and OM models on the shaking table are 0.31 g and 0.36 g, respectively. The macrocracks in the WRM and OM models rapidly expand in the peak acceleration interval of 0.3 to 0.5 g. Notably, the earthquake duration also has a significant effect on the extent of damage to concrete gravity dams under seismic action. When the ground-shaking PGA is large, the prolonged input ground shaking will lead to the deepening of cracks in the dam [33,34].

Figure 6 shows that the maximum tensile strains dramatically change on the downstream slope of the WRM-scaled model (points C and D) and the downstream slope of the guide wall of the OM-scaled model (point D) as the peak acceleration increases. The maximum tensile strains at point D of the WRM- and OM-scaled models exceed the peak strain of the ECM (0.0001) when the peak acceleration reaches approximately 0.25 g and 0.30 g, respectively. These peak accelerations are almost the same as those observed when the natural frequencies of the WRM- and OM-scaled models begin to change. For the reinforced and unreinforced monolith, the trends of the maximum tensile strain are similar. The maximum tensile strain of the reinforced monolith is reduced by approximately 8% more than that for the unreinforced monolith.

Figure 7 shows that macrocracks mainly form at the downstream slope of the WRM-scaled model and the downstream slope of the guide wall of the OM-scaled model. The damage distributions of WRM and OM were similar to those of WRM in the literature [8] and OM in the literature [31]. In the OM-scaled model, the expansion of the macrocracks in the reinforced monolith is less notable than that in the unreinforced monolith. In the WRM-scaled model, the number of macrocracks in the reinforced monolith is higher than that for the unreinforced monolith, which is the same as the results of the study in the literature [8]. The results indicate that the SR will reduce the depth of macrocracks, but increase the number of macrocracks. In addition, the SR makes the fracture region of the dam diffuse. Due to the low reinforcement ratio, whether the reinforcement is used in the dam structure has little impact on the test results of natural frequency and displacement, but has a great impact on the crack propagation [30,31].

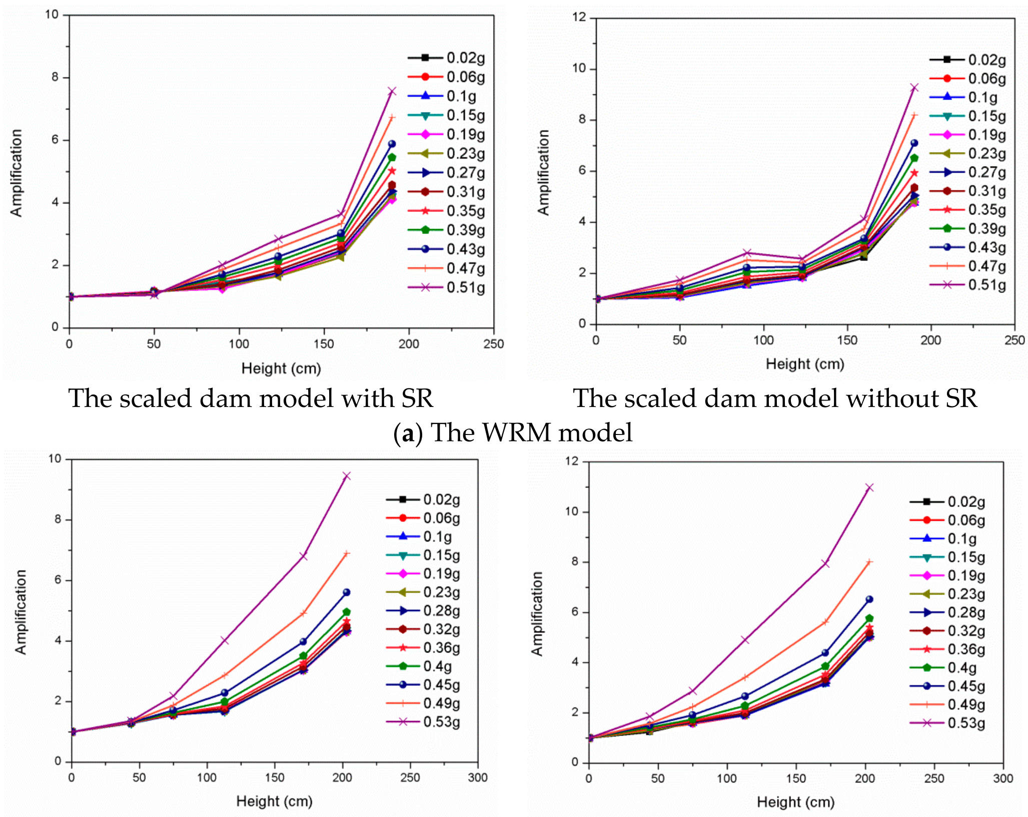

The scaled dam model with SR The scaled dam model without SR

(**a**) The WRM model

The scaled dam model with SR The scaled dam model without SR

(**b**) The OM model

Figure 5. The variation of acceleration amplification factor with height.

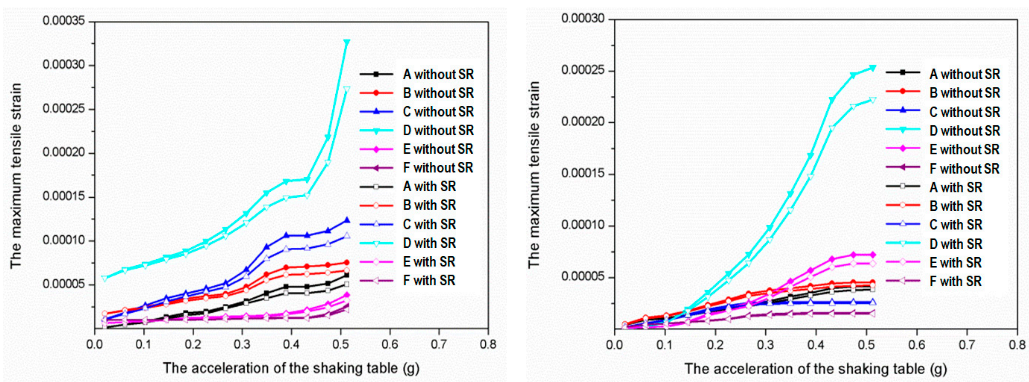

(**a**) The WRM model (**b**) The OM model

Figure 6. The maximum tensile strain of the model.

The cracks in the scaled dam model with SR

The cracks in the scaled dam model without SR

(**a**) The cracks in the WRM model

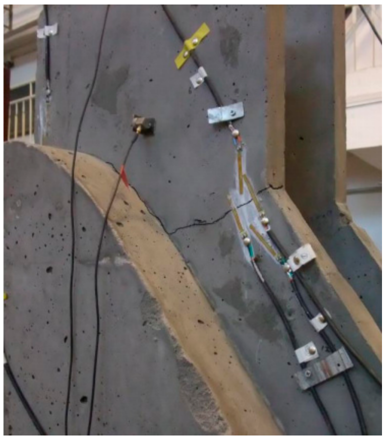

The cracks in the scaled dam model with SR

The cracks in the scaled dam model without SR

(**b**) The cracks in the OM model

Figure 7. The cracks in the scaled dam models.

3. The Numerical Simulation

3.1. Nonlinear Damage Constitutive Model for Concrete

The concrete damage model proposed by Lee and Fenves [11] is adopted, which is verified in reference [32]. Figure 8 shows the stress-strain relationship of concrete under uniaxial cyclic loading. For reinforced concrete materials, the constitutive relationship is described by Equation (17).

$$\sigma_S = \begin{cases} E_s\varepsilon,\ 0 < \varepsilon < \varepsilon_t \\ \frac{\kappa}{2}\left[\sqrt{(E_s\varepsilon)^2 + 4\alpha^2 f_{scr}^2} - E_s\varepsilon\right], & \varepsilon_t \le \varepsilon < \varepsilon_y \\ \kappa(f_y - E_s\varepsilon), & \varepsilon_y \le \varepsilon < \varepsilon_{sy} \\ 0, & \varepsilon_{sy} \le \varepsilon \end{cases} \tag{17}$$

where σ_s is the stress of reinforced concrete, ε and ε_t are the strain and the strain corresponding to tensile strength of concrete, respectively. E is the elastic modulus. The subscript s represents steel, and the subscript c represents concrete. $\kappa = \rho/(1-\rho)$, ρ is the ratio of reinforcement. ε_{sy} is the yield strain of steel.

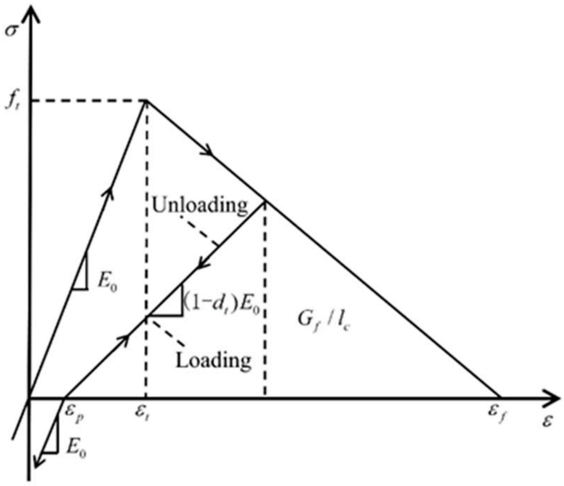

Figure 8. Stress-strain relationship of concrete under uniaxial cyclic loading.

The calculation of f_{scr} is shown in Equation (18).

$$f_{scr} = (1/\rho - 1 + E_s/E_c)f_t \tag{18}$$

where f is the strength of concrete, the subscript y represents steel, and the subscript t represents concrete.

Figure 9 is the stress-strain curve of reinforced concrete. The shadow part contributes to the stiffness of the tensile stiffener effect. Equation (19) is the stress-strain curve of reinforcement.

$$\sigma_S = \begin{cases} E_s\varepsilon_s & 0 \leq \varepsilon_s < \varepsilon_y \\ f_y & \varepsilon_s \geq \varepsilon_y \end{cases} \tag{19}$$

where σ_s, ε_s, ε_y, and E_s are the stress, strain, yield strain, and elastic modulus of steel, respectively, f_y is the yield strength of the steel.

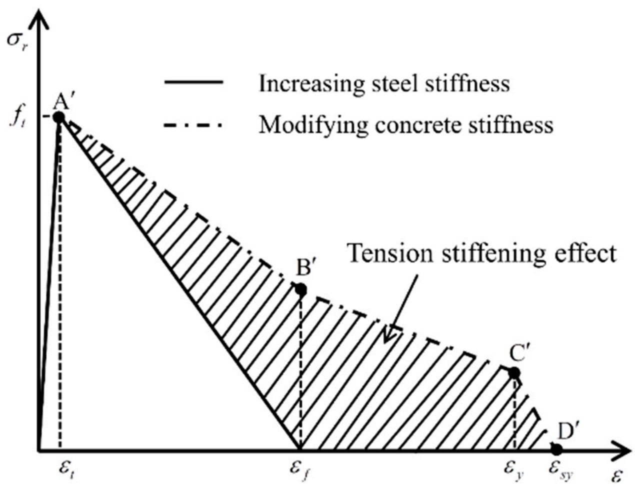

Figure 9. The stress-strain relationship of reinforced concrete.

3.2. Numerical Model of the Huangdeng Gravity Dam

The WRM and OM numerical models of the Huangdeng gravity dam were analyzed using the commercial finite element software ABAQUS. The element types and element numbers of the finite element model are shown in Figure 10. Some parameters of concrete and SR are given in the previous section. The damage parameters of the Huangdeng gravity dam model are as follows. The dilatancy angle is ψ = 36.31°. The fracture energy is G_f = 150 N/m. The density is ρ = 2400 kg/m^3. Additionally, the parameters of the SR of the gravity dam are as follows. The dynamic tensile strength of the SR is f_y = 300 MPa. The peak tensile strain is $\varepsilon_t = 0.101 \times 10^{-3}$. The whole reinforcement ratio of the dam is 0.04%, meeting the reinforcement requirements [35]. The limit strain of the concrete is $\varepsilon_f = 0.6 \times 10^{-3}$. The nominal strain is $\varepsilon_y = 1.3 \times 10^{-3}$. By using the Huangdeng gravity dam design response spectrum, artificial seismic acceleration loads were generated as the input to the numerical model, as shown in Figure 10. According to the results of Section 2, the peak horizontal acceleration required for rapid crack propagation in the dam is 0.5 g (a_r = 1). The peak input seismic acceleration is 0.5 g; the load input direction is horizontal and vertical. Since the shake table experiments do not consider the interaction between soil and foundation, the numerical model load input method is a rigid foundation inertia input. Furthermore, the equivalent Ghaemian radius of the cross-sectional area of beam elements is 0.05 m. Calculations were made for the dam with and without SR. Detailed material properties are given in reference [35]. The horizontal acceleration and frequency response of the top of the dam for the concrete gravity dam model are shown in Figure 11.

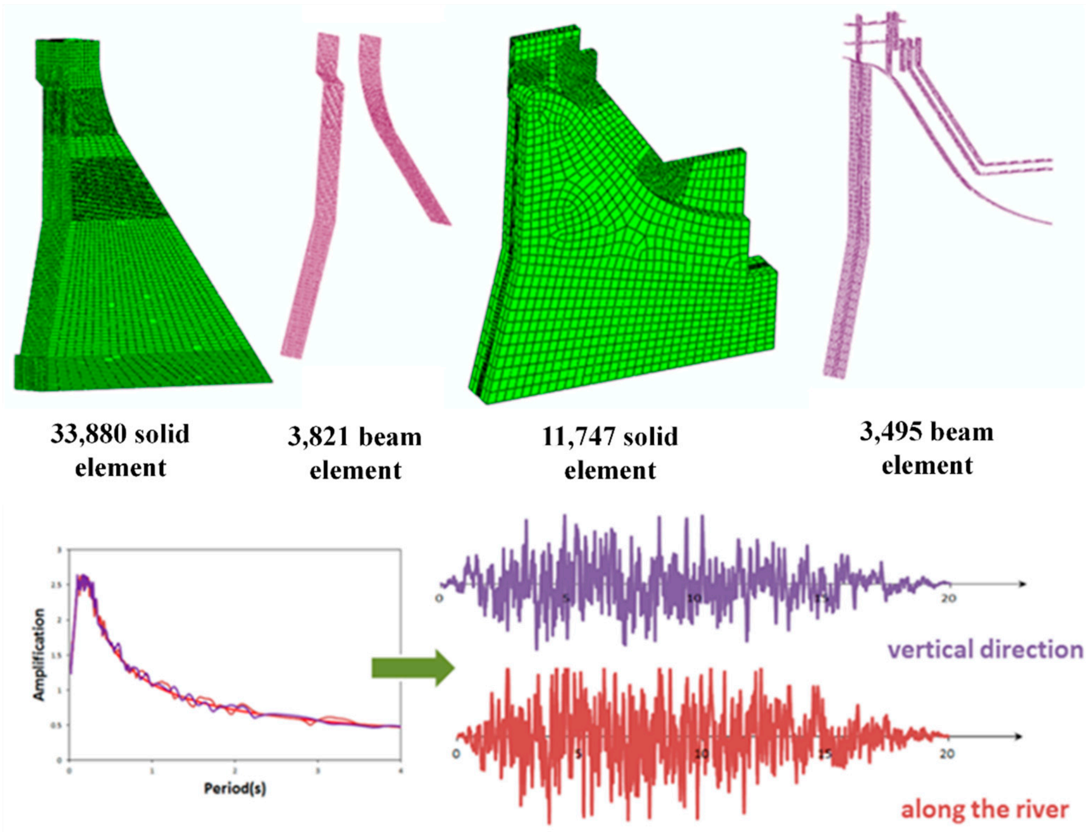

Figure 10. The element model of the Huangdeng gravity dam.

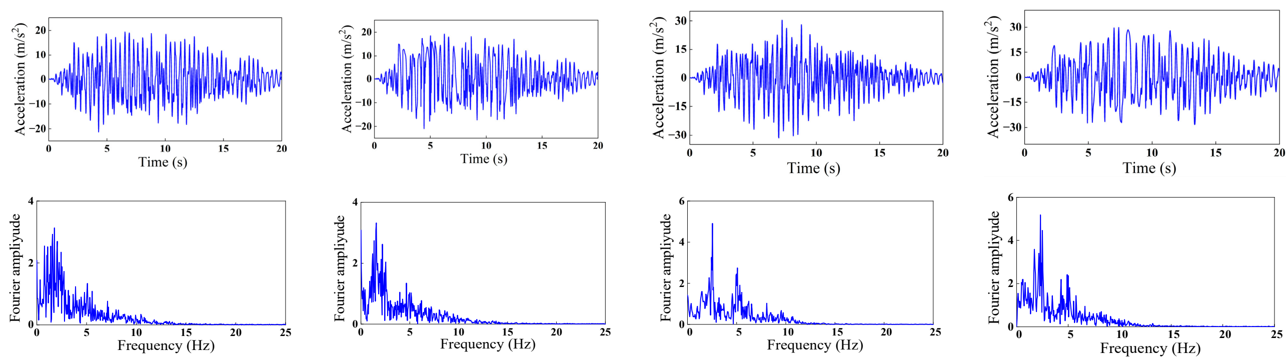

(**a**) WRM with SR (**b**) WRM without SR (**c**) OM with SR (**d**) OM without SR

Figure 11. Response signals in the time and frequency domains at the top of the numerical model.

3.3. Comparison Result of Numerical Model and Experimental Model

To verify the accuracy of the mechanical parameters of the experimental scale model, and according to the scaling rules of the mechanical parameters, the corresponding numerical model of the proportional model was established. Table 4 shows the results of the comparison between the natural frequencies of the numerical model of the scaled model and those of the experimental model. It can be found that f_{se} and f_{sn} are almost the same, which proves the correctness of the mechanical parameters of the experimental model.

In order to verify the accuracy of the numerical model, it is necessary to compare the experimental results with the numerical results. The natural frequencies of Huangdeng concrete gravity dam are given in Table 4 and are compared with the results of the shaking table test. It can be seen from Table 4 that the errors of f_{sc} and f_{pn} are within 5.5%, which basically meets the similarity constraint. The results show that the numerical model can accurately obtain the natural frequency of the structure, thus verifying the accuracy of the numerical model. Table 4 also shows that the natural frequencies of the reinforced WRM and OM models are 2.5% and 3.4% higher, respectively, than those of the unreinforced WRM and OM models. The results illustrate that the SR can improve the stiffness of the dam and reduce deformation. Figure 12 shows the vibration mode of the numerical simulation of the prototype structure of Huangdeng gravity dam. It can be seen that the SR has little influence on the dam's vibration mode.

Table 4. Comparison results of natural frequencies.

Monolith of the Dam	Natural Frequency f_{se} of the Scaled Experimental Model (Hz)	Conversion to the Natural Frequency f_{sc} of the Prototype by ω_r = 10 (Hz)	Natural Frequency f_{sn} of the Scaled Model Numerical Model (Hz)	Natural Frequency f_{pn} of the Dam Prototype Numerical Model (Hz)	Relative Error $\lvert f_{sc} - f_{pn} \rvert / f_{pn}$ (%)
WRM with SR	21.34	2.134	21.34	2.086	2.30
WRM without SR	20.80	2.080	20.48	2.047	1.61
OM with SR	16.87	1.687	16.88	1.782	5.33
OM without SR	16.31	1.631	16.34	1.602	1.81

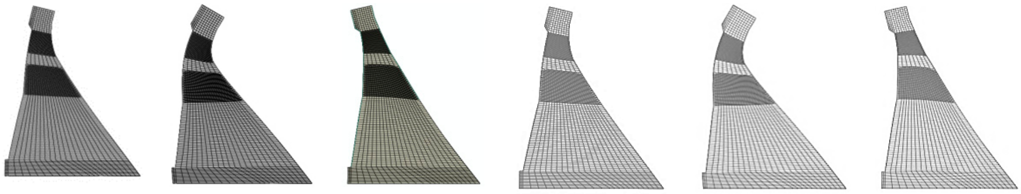

1st-order 2nd-order 3rd-order 1st-order 2nd-order 3rd-order

(**a**) The first-order to third-order vibration modes of the WRM with SR (**b**) The first-order to third-order vibration modes of the WRM without SR

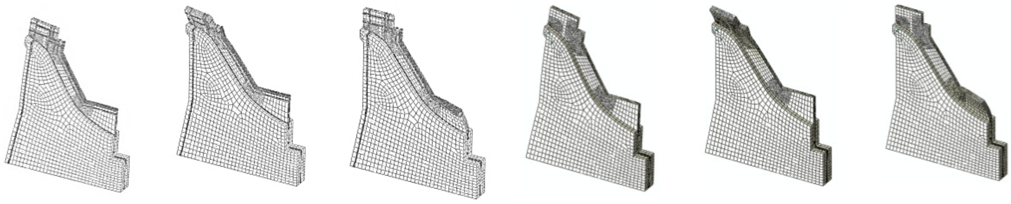

1st-order 2nd-order 3rd-order 1st-order 2nd-order 3rd-order

(**c**) The first-order to third-order vibration modes of the OM with SR (**d**) The first-order to third-order vibration modes of the OM without SR

Figure 12. The vibration modes of the prototype numerical model.

3.4. The Damage and Stress Results

Figure 13 shows the damage distribution of the dam numerical model. It can be seen that the structure is mainly damaged on the downstream slope of the WRM and the downstream slope of the guide wall of the OM. For the OM, the damage depth and damage magnitude of the reinforced monolith are obviously smaller than those for the unreinforced monolith. For the WRM, the damage to the reinforced monolith tends to diffuse. These prototype numerical results are similar to the scaled experimental results.

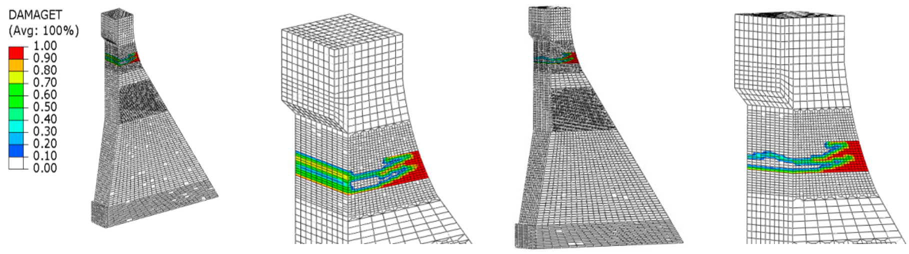

(**a**) The damage distribution for the WRM with SR (**b**) The damage distribution for the WRM without SR

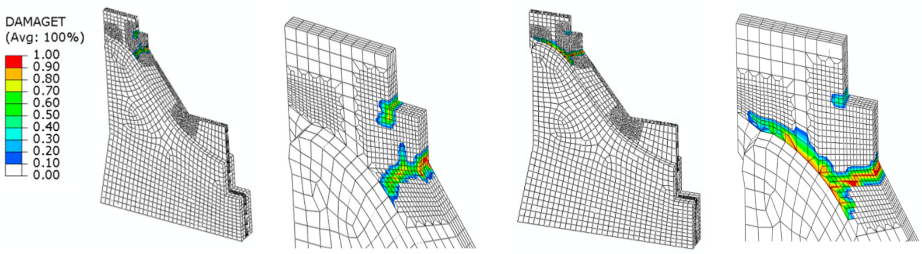

(**c**) The damage distribution for the OM with SR (**d**) The damage distribution for the OM without SR

Figure 13. The damage distribution for the prototype numerical model.

Figure 14 shows that the maximum tensile stresses of WRM and OM at the dam heel, upstream slope, and downstream slope are larger. In addition, the maximum tensile stress near the damage region is relatively small compared to that in other areas. These results illustrate that the tensile stress in the dam concrete near the damage region is released as the damage region expands. According to the above results, the tensile stress of dam concrete near the damage area is released with the expansion of the damage area.

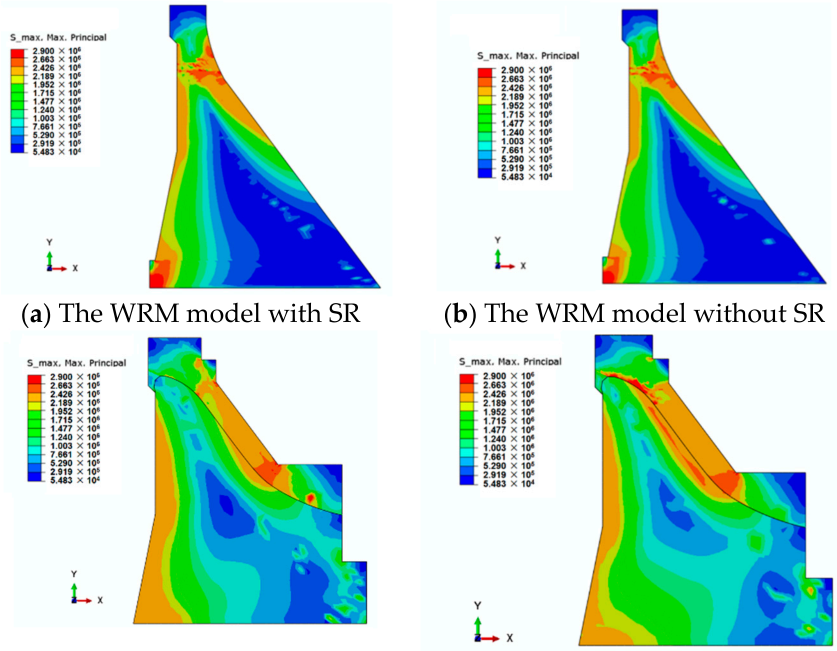

(**a**) The WRM model with SR (**b**) The WRM model without SR

(**c**) The OM model with SR (**d**) The OM model without SR

Figure 14. The maximum tensile stress in the concrete of Huangdeng dam.

Figure 15 shows that the maximum tensile stress on the SR increases as the damage region expands. The trends of the maximum tensile stress for the SR and dam concrete are opposed, mainly due to the relationship between the tensile stress of the SR and the crack opening process in the dam concrete. The extensive damage leads to the development of large cracks in the dam concrete. Thus, the maximum tensile stress of the SR will increase.

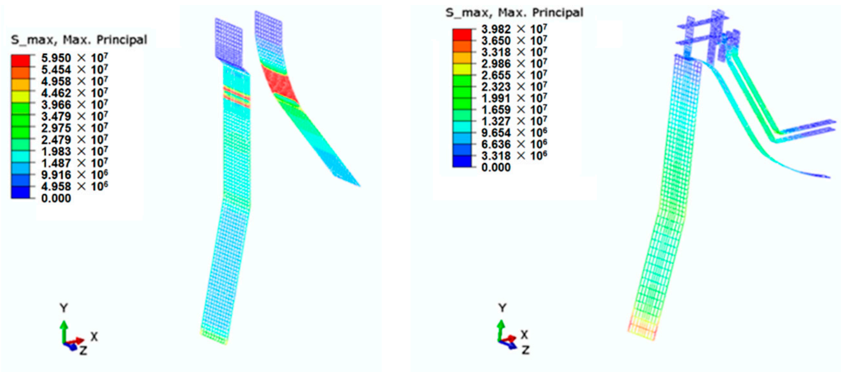

(**a**) The WRM model (**b**) The OM model

Figure 15. The maximum tensile stress on the SR of Huangdeng dam.

4. Conclusions

Through shaking table model tests and numerical simulations of reinforced and unreinforced WRMs and OMs of the Huangdeng concrete gravity dam, the following conclusions were obtained.

(1) The similarity relation of SR was derived based on the similarity relation of the prototype and scale model of the dam, which neglected the inertia scale of the steel reinforcement. Accurate intrinsic frequencies could be obtained using the proposed

SR similarity requirement and other similarity laws. In addition, the results of the prototype numerical calculations were similar to the results of the scalar experiments in terms of damage. It indicated that the SR similarity relationship derived in this paper could accurately reflect the true reinforcement morphology of the structure and could be used in shaking table experimental studies of reinforced concrete gravity dams.

(2) The peak accelerations associated with the appearance of microcracks in the WRM and OM were approximately 0.25 g and 0.30 g, respectively. Additionally, the peak accelerations associated with the appearance of macrocracks in the WRM and OM were 0.31 g and 0.36 g, respectively. The macrocracks in the WRM and OM rapidly expanded in the peak acceleration interval of 0.3 to 0.5 g. The aseismic stability of the OM was higher than that of the WRM.

(3) The role of SR was mainly in preventing macrocracks from extending, and the SR had little effect on microcrack formation. The SR reduced the depth of macrocracks, the damage depth, and the damage magnitude, but increased the number of macrocracks. In addition, the SR caused the fracture and damage regions of the dam to diffuse. The SR could improve the stiffness of the dam and reduce deformation. However, the SR had little effect on the dam's vibration mode.

(4) Crack propagation in the dam led to changes in the natural frequencies and distribution of amplification with height. The tensile stress in the dam concrete near the damage region was relatively small compared to that in other areas of the dam. The tensile stress on the SR increased as the damage region expanded. Tensile stress trends for the SR and dam concrete were opposed.

In conclusion, this research provides a rational foundation for further study of the similarity laws for reinforced dams.

Author Contributions: Conceptualization, methodology, formal analysis, writing—original draft preparation, software, data curation, Q.X. and B.L.; validation, writing—review and editing, J.C.; validation, funding acquisition, B.L., Q.X., J.C., M.W. and J.L. All authors have read and agreed to the published version of the manuscript.

Funding: This work is financially supported by the National Natural Science Foundation of China (Grant Nos. 52192672 and 52079025). These sources of financial support are gratefully acknowledged.

Data Availability Statement: The data presented in this study are available on request from the corresponding author.

Conflicts of Interest: The authors declare no conflict of interest.

References

1. Harris, D.W.; Snorteland, N.; Dolen, T.; Travers, F. Shaking table 2-d models of a concrete gravity dam. *Earthq. Eng. Struct. D* **2000**, *29*, 769–787. [CrossRef]
2. Ghobarah, A.; Ghaemian, M. Experimental study of small scale dam models. *J. Eng. Mech.* **1998**, *124*, 1241–1248. [CrossRef]
3. Donlon, W.; Hall, J.F. Shaking table study of concrete gravity dam monoliths. *Earthq. Eng. Struct. D* **1991**, *20*, 769–786. [CrossRef]
4. Aldemir, A.; Binici, B.; Arici, Y.; Kurc, O.; Canbay, E. Pseudo-dynamic testing of a concrete gravity dam. *Earthq. Eng. Struct. D* **2015**, *44*, 1747–1763. [CrossRef]
5. Phansri, B.; Charoenwongmit, S.; Yooprasertchai, E.; Park, K.H.; Warnitchai, P.; Shin, D.H. An experimental study on shaking table tests on models of a concrete gravity dam. *KSCE J. Civ. Eng.* **2015**, *19*, 142–150. [CrossRef]
6. Ghaemmaghami, A.R.; Ghaemian, M. Shaking table test on small-scale retrofitted model of Sefid-rud concrete buttress dam. *Earthq. Eng. Struct. D* **2010**, *39*, 109–118. [CrossRef]
7. Zhao, R. Experimental and Numerical Study of RCC Dams Strengthened with Reinforcement in Monolith for Seismic Resistance. Ph.D. Thesis, Dalian University of Technology, Dalian, China, 2007. (In Chinese).
8. Wang, M.M.; Chen, J.Y.; Fan, S.L. Experimental study on high gravity dam strengthened with reinforcement for seismic resistance on shaking table. *Struct. Eng. Mech.* **2014**, *51*, 663–683. [CrossRef]
9. Pilarska, D.; Maleska, T. Numerical Analysis of Steel Geodesic Dome under Seismic Excitations. *Materials* **2021**, *14*, 4493. [CrossRef]
10. Tran, N.X.; Gu, K.Y.; Yoo, M.; Kim, S.R. Numerical evaluation of slope effect on soil–pile interaction in seismic analysis. *Appl. Ocean Res.* **2022**, *126*, 103291. [CrossRef]

11. Wu, D.; Jiang, D.; Zhao, B. Nonlinear numerical modeling approach and seismic mechanism analysis on new modular precast composite shear wall structure. *Eng. Struct.* **2022**, *270*, 114868. [CrossRef]
12. Pekau, O.A.; Feng, L.M.; Zhang, C.H. Seismic fracture of Koyna dam: Case study. *Earthq. Eng. Struct. D* **1995**, *24*, 15–33. [CrossRef]
13. Ayari, M.L.; Saouma, V.E. A fracture mechanics based seismic analysis of concrete gravity dams using discrete cracks. *Eng. Fract. Mech.* **1990**, *35*, 587–598. [CrossRef]
14. Lee, J.; Fenves, G.L. A plastic-damage concrete model for earthquake analysis of dams. *Earthq. Eng. Struct. D* **1998**, *27*, 937–956. [CrossRef]
15. Bhattacharjee, S.S.; Leger, P. Seismic cracking and energy dissipation in concrete gravity dams. *Earthq. Eng. Struct. D* **1993**, *22*, 991–1007. [CrossRef]
16. Calayir, Y.; Karaton, M. A continuum damage concrete model for earthquake analysis of concrete gravity dam–reservoir systems. *Soil Dyn. Earthq. Eng.* **2005**, *25*, 857–869. [CrossRef]
17. Kuhl, E.; Ramm, E.; de Borst, R. An anisotropic gradient damage model for quasi-brittle materials. *Comput. Methods Appl. Mech. Eng.* **2000**, *183*, 87–103. [CrossRef]
18. Valliappan, S.; Yazdchi, M.; Khalili, N. Earthquake analysis of gravity dams based on damage mechanics concept. *Int. J. Numer. Anal. Methods Geomech.* **1996**, *20*, 725–751. [CrossRef]
19. Horii, H.; Chen, S. Computational fracture analysis of concrete gravity dams by crack-embedded elements-toward an engineering evaluation of seismic safety. *Eng. Fract. Mech.* **2003**, *70*, 1029–1045. [CrossRef]
20. Pekau, O.A.; Cui, Y. Failure analysis of fractured dams during earthquakes by DEM. *Eng. Struct.* **2004**, *26*, 1483–1502. [CrossRef]
21. Maclaughlin, M.M.; Doolin, D.M. Review of validation of the discontinuous deformation analysis (DDA) method. *Int. J. Numer. Anal. Methods Geomech.* **2006**, *30*, 271–305. [CrossRef]
22. Zhu, W.; Tang, C. Numerical simulation on shear fracture process of concrete using mesoscopic mechanical model. *Constr. Build. Mater.* **2002**, *16*, 53–463. [CrossRef]
23. Long, Y.; Zhang, C.; Jin, F. Numerical simulation of reinforcement strengthening for high-arch dams to resist strong earthquakes. *Earthq. Eng. Struct. D* **2008**, *37*, 1739–1761. [CrossRef]
24. Gilbert, R.I.; Warner, R.F. Tension stiffening in reinforced concrete slabs. *ACSE J. Struct. Eng.* **1978**, *104*, 1885–1901. [CrossRef]
25. An, X.; Maekawa, K.; Okamura, H. Numerical simulation of size effect in shear strength of RC beams. *Doboku Gakkai Ronbunshu* **1997**, *564*, 297–316. [CrossRef]
26. Hariri-Ardebili, M.A.; Seyed-Kolbadi, S.M. Seismic cracking and instability of concrete dams: Smeared crack approach. *Eng. Fail. Anal.* **2015**, *52*, 45–60. [CrossRef]
27. Zhong, H.; Lin, G.; Li, X.; Li, J. Seismic failure modeling of concrete dams considering heterogeneity of concrete. *Soil Dyn. Earthq. Eng.* **2011**, *31*, 1678–1689. [CrossRef]
28. Philippe, B.M.; Pierre, L.; Rene, T. Seismic behavior of post-tensioned gravity dams: Shake table experiments and numerical simulations. *J. Struct. Eng.* **2002**, *128*, 140–152.
29. Fan, S.; Chen, J.; Wang, J.; Zhong, H. Experimental study and numerical simulation for seismic failure of high arch dam on shaking table. *Chin. J. Rock Mech. Eng.* **2009**, *28*, 467–474.
30. Xu, Q.; Chen, J.; Liu, B.; Li, J. Investigation of Non-fully Similar Laws of Damage to an Arch Dam in Shaking Table Model Tests. *Adv. Mech. Eng.* **2020**, *12*, 168781402097449. [CrossRef]
31. Wang, M.M.; Chen, J.Y.; Wei, H.; Song, B. Experimental investigation of a small-scaled model for overflow section of a high gravity dam on shaking table. *Adv. Mech. Eng.* **2019**, *11*, 1687814019829959. [CrossRef]
32. *NB 35047-2015*; NB 35047-2015 Code for Seismic Design of Hydraulic Structures of Hydropower Project. National Energy Board of China: Beijing, China, 2012. (In Chinese)
33. Xu, B.; Wang, X.; Pang, R.; Zhou, Y. Influence of strong motion duration on the seismic performance of high CFRDs based on elastoplastic analysis. *Soil Dyn. Earthq. Eng.* **2018**, *114*, 438–447. [CrossRef]
34. Wang, G.; Zhang, S.; Zhou, C.; Lu, W. Correlation between strong motion durations and damage measures of concrete gravity dams. *Soil Dyn. Earthq. Eng.* **2015**, *69*, 148–162. [CrossRef]
35. Xu, Q.; Zhang, T.; Chen, J.; Li, J. The influence of reinforcement strengthening on seismic response and index correlation for high arch dams by endurance time analysis method. *Structures* **2021**, *32*, 355–379. [CrossRef]